Pre-Equalization for Pre-Rake DS-UWB Systems with Spectral Mask Constraints

Amir-Hamed Mohsenian-Rad, *Member, IEEE*, Jan Mietzner, *Member, IEEE*, Robert Schober, *Fellow, IEEE*, and Vincent W.S. Wong, *Senior Member, IEEE*

***Abstract*— In this paper, we propose a novel optimization-based pre-equalization filter (PEF) design framework for direct-sequence ultra-wideband (DS-UWB) systems with pre-Rake combining. The key feature in our design is that we explicitly take into account the *spectral mask* constraints that are usually imposed in practice by the telecommunications regulation and standardization bodies. This avoids the need for an inefficient *power back-off*, which is necessary for the existing pre-Rake-based transmitter structures designed solely based on average transmit power constraints. We consider two PEF design structures. In the first structure, the PEF is placed *before* the up-sampling unit at the transmitter. In the second structure, the PEF is placed *after* the up-sampling unit. We show that these two structures are significantly different in terms of their capabilities in reducing the residual inter-symbol interference at the receiver and also in following the spectral mask at the transmitter. This introduces a *trade-off* such that one design structure outperforms the other one, depending on the system parameters. In this regard, we show that if the spreading factor is large enough, the second design structure has a superior performance. Simulation results confirm that both of the proposed PEF structures lead to significant performance gains over PEF designs without explicit spectral mask considerations. In addition, our PEF designs have the capability of adhering to spectral masks with arbitrary shapes.**

***Index Terms*— Spectral mask constraints, pre-equalization, pre-Rake combining, ultra-wideband communication, inter-symbol interference, optimization, semi-definite programming.**

I. Introduction

Ultra-wideband (UWB) is an emerging technology for high-rate short-range transmission, e.g., in wireless personal area networks. Due to their extremely large bandwidth, both direct-sequence (DS) [1], [2] and impulse-radio (IR) [3], [4] UWB systems can resolve even dense multipath components such that Rake combining can be used at the receiver to significantly reduce the negative impacts of fading in the received signal [4]. However, for many UWB applications, the receiver is a portable device with severely limited signal processing capabilities, making the implementation of Rake combiners with a sufficiently large number of fingers very challenging.

To overcome this problem, a promising approach is to move computational complexity from the receiver to the more powerful transmitter (e.g., an access point). In this regard, *pre-Rake combining* can be used [5], [6]. It exploits the reciprocity of the UWB radio channel, which has recently been confirmed experimentally in [7]. Ideally, with pre–Rake combining at the transmitter, channel estimation, diversity combining, and equalization are not required at the receiver, and a simple symbol–by–symbol detector can be used [1], [6]. However, pre-Rake combining has several drawbacks. In particular, for *long* channel impulse responses (CIRs), which are typical for UWB applications, it may entail a relatively high error floor if simple symbol–by–symbol detection is applied at the receiver [8]. To remedy this problem, while keeping the receiver simple, *pre-equalization* can be used at the transmitter, possibly along with a pre-Rake combiner, to reduce the residual inter-symbol interference (ISI) at the receiver [9], [10].

Most of the previous work on UWB pre-Rake and pre-equalizer design (e.g., in [1], [5]–[10]) includes only constraints to limit the average transmit power. However, prior studies do not include constraints to limit the *power spectral density* (PSD) of the transmitted UWB signals. This can severely affect the overall system performance as most of the telecommunications regulation bodies, e.g., the US Federal Communications Commission (FCC), impose *spectral mask* constraints to limit UWB emission levels to prevent harmful interference on incumbent legacy narrow-band receivers. In such a setting, the existing UWB pre-filtering techniques can be far from optimal, as they require an appropriate *power back-off* so that the mandatory spectral masks are not violated.

In this paper, we propose two novel *pre-equalization filter* (PEF) designs with pre-Rake combining for DS-UWB systems. The two designs differ in where the PEF is located with respect to the up-sampling unit at the transmitter. The contributions of this paper can be summarized as follows.

- *New Problem Formulation*: For each design, we formulate an elaborate optimization problem, with the coefficients of the PEF being the optimization variables. Each optimization problem includes constraints with respect to the spectral mask, residual ISI, and the average transmit power. To the best of our knowledge, this work is the first to explicitly take into account spectral mask constraints for pre-equalization in UWB systems.
- *Efficient Algorithm Design*: Since the formulated optimization problems are *non-convex* and difficult to solve in general, we propose a simple algorithm based on a *semi-definite relaxation* technique in order to find close-to-optimal solutions for each PEF design problem.
- *Design Trade-off*: For the existing pre-filter designs *without* spectral mask consideration (cf. [9]), placing the PEF

Manuscript was received on November 22, 2009; revised on July 31, 2010; and accepted on October 7, 2010. This paper has been presented in part at the *IEEE ICC'10*, Cape Town, South Africa, May 2010.

A. H. Mohsenian-Rad is with the Department of Electrical and Computer Engineering, Texas Tech University, Lubbock, TX 79409, USA, e-mail: hamed.mohsenian@ttu.edu. This work was completed when he was with the Department of Electrical and Computer Engineering, University of British Columbia, Vancouver, BC, Canada, V6T 1Z4. J. Mietzner, R. Schober and V. W. S. Wong are with the Department of Electrical and Computer Engineering, University of British Columbia, Vancouver, BC, Canada, V6T 1Z4, e-mails: jan.mietzner@ieee.org and {rschober, vincentw}@ece.ubc.ca.

before the up-sampler can reduce the required length of the PEF. This is mainly due to a better residual ISI reduction. However, we will show in this paper that a PEF located before the up-sampling unit has major difficulties satisfying spectral mask constraints. This limits the achievable performance, particularly when the spreading factor is *large*. In fact, we will show that whether it is more beneficial to place the PEF before or after the up-sampling unit highly depends on the system parameters.

- *Improved Performance*: Simulation results confirm that our PEF designs lead to significant performance gains over PEF designs that do not take into account the spectral mask constraints. In particular, our designs outperform the PEF designs in [9] and [10].

Note that the PEF designs in this paper are different from the previous work in the literature on UWB *pulse-shaping* with spectral mask considerations, e.g. in [3], [11], which does not address pre-equalization as well as residual ISI suppression.

Organization: The system model is presented in Section II. We formulate the PEF optimization problems in Section III. An efficient algorithm to solve these problems is provided in Section IV. Simulation results are given in Section V. The paper is concluded in Section VI.

Notation: $\mathcal{E}\{\cdot\}$, $[\cdot]^T$, $(\cdot)^*$, $[\cdot]^H$, $\Re\{\cdot\}$, $\lceil\cdot\rceil$, $\delta(\cdot)$, and $*$ denote expectation, transposition, complex conjugation, Hermitian transposition, the real part of a complex number, the ceiling function, the Dirac delta function, and convolution, respectively. Also $X(e^{j\omega}) \triangleq \mathcal{F}\{x[k]\} = \sum_{k=-\infty}^{\infty} x[k]e^{-j\omega k}$, $X(j\Omega) \triangleq \mathcal{F}\{x(t)\} = \int_{-\infty}^{+\infty} x(t)e^{-j\Omega t}dt$, $\Phi_{xx}(e^{j\omega}) \triangleq \mathcal{F}\{\phi_{xx}[\tau]\} = \sum_{\tau=-\infty}^{\infty} \phi_{xx}[\tau]e^{-j\omega\tau}$, and $\phi_{xx}[\tau] \triangleq \mathcal{E}\{x[k]x^*[k-\tau]\}$ denote the *discrete–time* Fourier transform, the *continuous–time* Fourier transform, the power spectral density, and the autocorrelation function, respectively. Depending on the context, $x[n]$ represents either a sequence or the nth element of a sequence. When $x[n]$ is up-sampled by a factor of $N > 1$ it yields a new sequence $x^N[k]$ where $x^N[k] = x[n]$ if $k = Nn$ and $x^N[k] = 0$ if $k \neq Nn$.

II. System Model

In this section, we consider two DS-UWB transceiver structures, each one with a single transmit antenna and a single receive antenna as shown in the block diagrams in Fig. 1. Here, our system setup is similar to that in [2]. Next, we explain the details of the system model and the differences between the two design structures shown in Figs. 1(a) and (b). We denote the symbol duration by T_s and the chip duration by $T_c = T_s/N$, where N is the *spreading factor*. All signals and systems are represented in complex baseband.

A. Transmitter Structure I

Consider the DS-UWB system block diagram in Fig. 1(a). At the transmitter, a sequence of independent and identically distributed (i.i.d.) data symbols $a[n] \in \{\pm 1\}$ is filtered with PEF $f_1[n]$ of length L_f, and the filter output signal is obtained as

$$v_1[n] \triangleq f_1[n] * a[n] = \sum_{l=0}^{L_f-1} f_1[l]a[n-l]. \qquad (1)$$

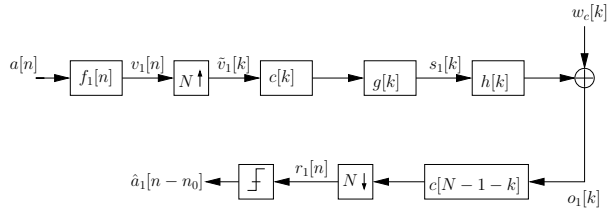

(a) Structure I: Pre-equalization filter is placed *before* the up-sampler.

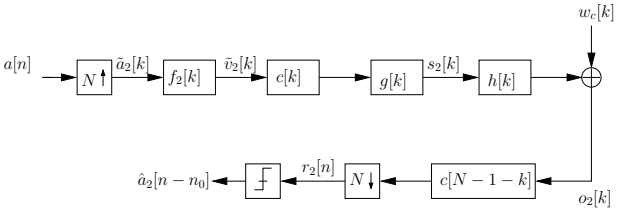

(b) Structure II: Pre-equalization filter is placed *after* the up-sampler.

Fig. 1. Block diagrams of the two UWB structures studied in this paper. Each structure includes one transmit antenna, pre-equalization, pre-Rake combining, and one receive antenna. The two transceiver structures differ in where the PEF is located with respect to the up-sampling unit at the transmitter. The receiver has minimal complexity in both structures. Only a simple –by–symbol detector is used at the receiver in both Structures I and II.

We will optimize the PEF to minimize the residual ISI at the receiver in Sections III and IV. Here, we place the PEF *before* the up-sampling unit. It is shown in [9] that for the case *without* spectral mask constraints, this structure can reduce the required length of the PEF. The output signal of the PEF is *up-sampled* by a factor of $N \geq 1$ to yield $\tilde{v}_1[k] \triangleq v_1^N[k]$. Sequence $\tilde{v}_1[k]$ is then filtered with a (real-valued) spreading sequence $c[k]$, $0 \leq k < N$, which is normalized such that $\sum_{k=0}^{N-1} |c[k]|^2 = 1$, and a pre-Rake filter $g[k]$ of length L_g. The resulting transmit sequence $s_1[k]$ is given by

$$s_1[k] = \tilde{v}_1[k] * \tilde{g}[k] = \sum_{i=-\infty}^{\infty} v_1[i]\tilde{g}[k-iN], \qquad (2)$$

where

$$\tilde{g}[k] \triangleq c[k] * g[k] = \sum_{i=0}^{N-1} c[i]g[k-i] \qquad (3)$$

includes the combined effects of the pre-Rake filter $g[k]$ and spreading sequence $c[k]$. Here, we consider a general transmitter structure as we do not impose any restrictions on $c[k]$ and $g[k]$. If a spreading sequence is not applied, e.g. as in [5]–[7], we simply have $c[0] = 1$ and $c[k] = 0$, $1 \leq k < N$. In general, $g[k]$ depends in some way on the CIR $h[k]$, which has length L_h. In an *all-pre-Rake* (also called *time-reversal*) filter, we have [5]

$$g[k] \triangleq h^*[L_h - k - 1], \quad 0 \leq k < L_g, \quad L_g = L_h. \qquad (4)$$

B. Transmitter Structure II

Next, we consider the second DS-UWB transceiver structure shown in Fig. 1(b). Unlike the case for the first structure in Fig. 1(a), here the PEF is placed *after* the up-sampling unit. We will show in Section V that in most practical cases, particularly when the PEF filter length L_f and the spreading factor N are not too small, Structure II can significantly outperform

Structure I due to an improved capability of conforming to the spectral mask constraints. According to the second design structure in Fig. 1(b), at the transmitter a sequence of i.i.d. data symbols $a[n] \in \{\pm 1\}$ is first up-sampled by a factor of $N \geq 1$ to yield $\tilde{a}_2[k] \triangleq a_2^N[k]$. It is then, respectively, filtered with a PEF $f_2[k]$ of length L_f, spreading sequence $c[k]$ of length N, and pre-Rake-combining filter $g[k]$ of length L_g. The resulting transmit sequence $s_2[k]$ is given by

$$s_2[k] = \tilde{a}_2[k] * f_2[k] * \tilde{g}[k], \tag{5}$$

where $\tilde{g}[k]$ is as in (3) and includes the combined effects of the pre-Rake filter and spreading.

C. Channel Model

The equivalent baseband discrete-time CIR

$$h[k] \triangleq g_T(t) * h(t) * g_R(t)|_{kT_c} \tag{6}$$

contains the combined effects of a square-root Nyquist transmit filter $g_T(t)$ [2], the continuous-time CIR $h(t)$, and the receive filter $g_R(t)$, sampled at chip interval T_c. For the wireless channel, we adopt the IEEE 802.15.3a channel model [12], [13]. Consequently, the passband version $h'(t)$ of the baseband CIR $h(t)$ consists of L_c clusters of L_r rays and is modeled as

$$h'(t) = \vartheta \sum_{l=1}^{L_c} \sum_{k=1}^{L_r} \rho_{k,l} \delta(t - T_l - \tau_{k,l}), \tag{7}$$

where T_l is the delay of the lth cluster, $\tau_{k,l}$ is the delay of the kth ray of the lth cluster, $\rho_{k,l}$ is the random multipath gain coefficient, and ϑ models the lognormal shadowing. In [12], [13], four parameter sets for the various channel model (CM) parameters in (7) are specified. The resulting channel models are known as CM1, CM2, CM3, and CM4. They represent different usage scenarios and entail different amounts of ISI.

D. Receiver Structure I

The received signal is obtained as

$$o_1[k] = \sum_{l=0}^{L_h-1} h[l] s_1[k-l] + w_c[k], \tag{8}$$

where $w_c[k]$ denotes the *chip-level* additive white Gaussian noise (AWGN) with variance $\sigma_c^2 \triangleq \mathcal{E}\{|w_c[k]|^2\}$. Received signal $o_1[k]$ is filtered with the *time-reversed* spreading sequence $c[N-1-k]$, $0 \leq k < N$, and is *down-sampled* at times $k = Nn + k_0$, where $0 \leq k_0 < N$ denotes the sampling phase. The resulting receiver output signal $r_1[n]$ can be expressed as

$$r_1[n] = \sum_{l=-\infty}^{\infty} q[Nl + k_0] v_1[n-l] + w_s[n], \tag{9}$$

with *overall* CIR

$$q[k] = \tilde{g}[k] * \tilde{h}[k] = \sum_{i=0}^{L_g+N-2} \tilde{g}[i] \tilde{h}[k-i] \tag{10}$$

and *symbol-level* noise

$$w_s[n] = \sum_{i=0}^{N-1} c[i] w_c[N(n-1) + k_0 + i + 1]. \tag{11}$$

Here, $\tilde{h}[k]$ includes the combined effects of the channel filter $h[k]$ and the time-reversed spreading sequence $c[N-1-k]$:

$$\tilde{h}[k] \triangleq h[k] * c[N-1-k] = \sum_{i=0}^{N-1} c[i] h[k+i-(N-1)]. \tag{12}$$

Note that $w_s[n]$ is also AWGN noise with variance $\sigma_s^2 \triangleq \mathcal{E}\{|w_s[n]|^2\} = \sigma_c^2 \sum_{i=0}^{N-1} |c[i]|^2 = \sigma_c^2$.

Since our goal is to design a UWB system with *minimal receiver complexity*, no additional filtering is applied at the receiver, and symbol decisions are made according to

$$\hat{a}_1[n - n_0] = \text{sign}\{\Re\{r_1[n]\}\}, \tag{13}$$

where $\hat{a}_1[n-n_0]$ is the estimate for $a[n-n_0]$ in Structure I, n_0 is decision delay, and $\text{sign}\{x\} = 1$ if $x \geq 0$ and $\text{sign}\{x\} = -1$ otherwise. Note that *no* equalizer is used at the receiver.

E. Receiver Structure II

The received signal is obtained as

$$o_2[k] = \sum_{l=0}^{L_h-1} h[l] s_2[k-l] + w_c[k]. \tag{14}$$

Applying (5) in (14), the resulting receiver output signal $r_2[n]$ can be expressed as

$$r_2[n] = \sum_{l=-\infty}^{\infty} b[Nl + k_0] a[n-l] + w_s[n], \tag{15}$$

where

$$b[k] \triangleq f_2[k] * q[k] = \sum_{i=0}^{L_f-1} f_2[i]\, q[k-i] \tag{16}$$

with overall CIR $q[k]$ as in (10) and symbol-level noise $w_s[n]$ as in (11). At the receiver, the symbol decisions are made as $\hat{a}_2[n - n_0] = \text{sign}\{\Re\{r_2[n]\}\}$, similar to (13) in Structure I.

III. Formulation of PEF Design Optimization Problems

In this section, we propose an optimization framework for the design of efficient PEFs with explicit spectral mask and various other design considerations. The proposed framework is applicable to both Structures I and II shown in Figs. 1(a) and (b). We will provide an algorithm to solve the optimization problems formulated in this section in Section IV.

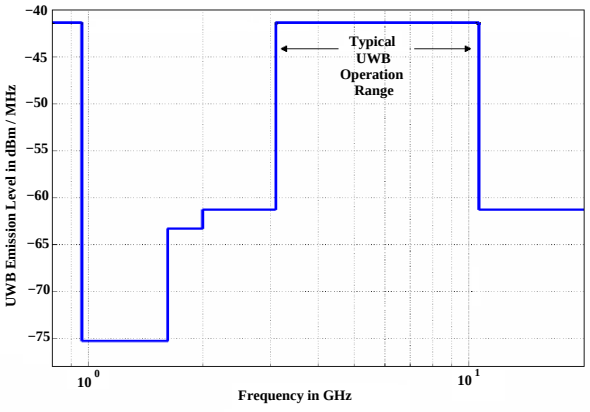

Fig. 2. FCC spectral mask for UWB transmissions in outdoor environment. A typical operation range for UWB systems is the 3.1-10.6 GHz band.

A. Problem Formulation for Structure I

Consider Structure I in Fig. 1(a). It is convenient to first rewrite (9) in vector form as

$$r_1[n] = (\mathbf{Q}\,\mathbf{f}_1)^H \mathbf{a}[n] + w_s[n], \tag{17}$$

where

$$\mathbf{a}[n] \triangleq [a[n] \ \ldots \ a[n-L_t+1]]^T, \qquad \mathbf{f}_1 \triangleq [f_1[0] \ \ldots \ f_1[L_f-1]]^H, \tag{18}$$

and $\mathbf{Q}$ is an $L_t \times L_f$ *column-circulant* matrix with vector

$$[q[k_0] \ q[N+k_0] \ \ldots \ q[N(L_q-1)+k_0] \ \mathbf{0}_{L_f-1}^T]^H$$

as its first column. Here, $\mathbf{0}_{L_f-1}$ denotes an $(L_f-1)\times 1$ vector with all entries equal to zero, and

$$L_t \triangleq L_q+L_f-1 \qquad \text{and} \qquad L_q \triangleq \lceil (L_g+L_h+2N-3)/N \rceil \tag{19}$$

are the lengths of the impulse response of the overall system (including the PEF) and the sampled overall CIR $q[Nn+k_0]$, respectively. Next, we study PEF design aspects.

1) Spectral Mask Constraints: The telecommunications regulation and standardization bodies, such as the FCC in the US, impose regulations which limit the permitted PSD for UWB transmissions to prevent interference to incumbent legacy narrow-band receivers. The FCC *spectral mask* for outdoor communications is shown in Fig. 2 [14].[1]

We first note that our system model is in *discrete–time*, while the spectral masks are usually defined in *continuous–time*. Let Ω and ω denote the angular frequencies associated with the continuous–time and discrete–time Fourier transform, respectively. We define $\Omega_{\min}$ and $\Omega_{\max}$ as the minimum and maximum frequencies used by the UWB system (e.g., $\Omega_{\min} = 2\pi \times 3.5$ GHz and $\Omega_{\max} = 2\pi \times 4.5$ GHz [2]).

[1]In addition to the spectral mask constraint, the FCC has also issued a peak power constraint in time domain. As shown in [15], for IR-UWB systems with small pulse rates (corresponding to DS-UWB systems with relatively large spreading factors), the peak power constraint in time domain is the binding one, whereas for high-rate IR-UWB systems (or DS-UWB systems with moderate spreading), it is the spectral mask constraint which is binding. For practical relevance, we focus on the latter case. For example, given a system bandwidth of 1 GHz, DS-UWB systems with spreading factors $N \leq 50$ are well within the regime where the spectral mask constraint is binding.

Let $B_s = \Omega_{\max} - \Omega_{\min}$ denote the total bandwidth used by the designed UWB system. Also let $m(\Omega)$ denote the spectral mask (e.g., $m(\Omega) = -41.3$ dBm/MHz for any $\Omega_{\min} \leq \Omega \leq \Omega_{\max}$ which is set by FCC). According to the FCC, the radiated emissions are measured at a *resolution bandwidth* of 1 MHz [14]. Therefore, we need to assure obeying the spectral mask within every 1 MHz of occupied bandwidth. Let $\Omega_1, \ldots, \Omega_K$ denote $K \triangleq \frac{B_s}{2\pi\times 1\text{MHz}} + 1$ discrete frequency levels which uniformly spread out over the bandwidth B_s. Clearly, $\Delta\Omega = \Omega_2 - \Omega_1 = \ldots = \Omega_K - \Omega_{K-1} = 2\pi \times 1$ MHz. For each $\mu = 1, \ldots, K$, it is required that [14]

$$\int_{\omega_\mu - \frac{\Delta\omega}{2}}^{\omega_\mu + \frac{\Delta\omega}{2}} \left| G_T\left(j\,\frac{\omega}{T_c}\right)\right|^2 \Phi_{s_1 s_1}(e^{j\omega}) d\omega \leq \int_{\Omega_\mu - \frac{\Delta\Omega}{2}}^{\Omega_\mu + \frac{\Delta\Omega}{2}} m(\Omega)\ d\Omega, \tag{20}$$

where $\omega_\mu \triangleq T_c\,\Omega_\mu$ [16, Ch. 1.7], $\Delta\omega \triangleq T_c\,\Delta\Omega$, $G_T(j\,\frac{\omega}{T_c}) = \mathcal{F}\{g_T(t)\}$, and $\Phi_{s_1 s_1}(e^{j\omega})$ denotes the PSD for transmitted signal $s_1[k]$. Recall that $g_T(t)$ is the transmit filter. We can show that

$$\Phi_{s_1 s_1}(e^{j\omega}) = \left|\tilde{G}(e^{j\omega})\right|^2\ \Phi_{\tilde{v}_1\tilde{v}_1}(e^{j\omega}), \tag{21}$$

where $\tilde{G}(e^{j\omega}) = \mathcal{F}\{\tilde{g}[k]\}$. We also have

$$\Phi_{\tilde{v}_1\tilde{v}_1}(e^{j\omega}) = \left|F_1(e^{j\omega N})\right|^2\ \Phi_{aa}(e^{j\omega N}) = \left|F_1(e^{j\omega N})\right|^2, \tag{22}$$

where $F_1(e^{j\omega N}) = \sum_{k=0}^{L_f-1} f_1[k] e^{-j\omega N k}$ and $\Phi_{aa}(e^{j\omega N}) = 1$ due to the i.i.d. assumption for the data symbols $a[n]$. From (21) and (22), and assuming that the spectral mask $m(\Omega)$ and PSD $|G_T(j\,\frac{\omega}{T_c})|^2\ \Phi_{s_1 s_1}(e^{j\omega})$ are practically constant over $\Omega_\mu - \frac{\Delta\Omega}{2} \leq \Omega \leq \Omega_\mu + \frac{\Delta\Omega}{2}$ and $\omega_\mu - \frac{\Delta\omega}{2} \leq \omega \leq \omega_\mu + \frac{\Delta\omega}{2}$, respectively, for each $\mu = 1, \ldots, K$, inequality (20) becomes

$$\lambda(\omega_\mu)\left|F_1(e^{j\omega_\mu N})\right|^2 \ \leq\ m(\Omega_\mu), \tag{23}$$

where

$$\lambda(\omega_\mu) \triangleq T_c\ \left|\tilde{G}(e^{j\omega_\mu})\right|^2\ \left|G_T\left(j\,\frac{\omega_\mu}{T_c}\right)\right|^2. \tag{24}$$

Clearly, we can ensure (23) by tuning the coefficients in the PEF, i.e., $f_1[0], \ldots, f_1[L_f-1]$. The spectral mask constraints in (23) can be written in vector form, using

$$\left|F_1(e^{j\omega N})\right|^2 = \mathbf{f}_1^H\ \mathbf{d}(N\omega)\ \mathbf{d}^H(N\omega)\ \mathbf{f}_1, \tag{25}$$

where $\mathbf{d}(N\omega) \triangleq [1 \ e^{j\omega N} \ e^{j\omega 2N} \ \ldots \ e^{j\omega(L_f-1)N}]^T$. Therefore, the spectral mask in (23) imposes K inequality constraints on the PEF coefficients $\mathbf{f}_1$ as

$$\lambda(\omega_\mu)\ \mathbf{f}_1^H\ \mathbf{d}(N\omega_\mu)\ \mathbf{d}^H(N\omega_\mu)\ \mathbf{f}_1 \leq m(\Omega_\mu), \quad \mu = 1, \ldots, K. \tag{26}$$

Note that $\lambda(\omega_\mu)$ is *fixed* for each $\mu = 1, \ldots, K$ as far as the design of the PEF is concerned.

2) Energy Concentration: Since we assume that *no* equalizer is used at the receiver, it is required that for each received symbol, most of the channel energy is concentrated in a *single* channel tap. Considering (17), let $\mathbf{Q}_{pre}$ denote the submatrix of $\mathbf{Q}$ consisting of the first η_{pre} rows. Also let $\mathbf{Q}_{post}$ denote the submatrix of $\mathbf{Q}$ consisting of the last η_{post} rows. Here,

η_{pre} and η_{post} are selected such that $\eta_{pre} + \eta_{post} + 1 = L_t$, where L_t is as in (19). We can rewrite $\mathbf{Q}$ as

$$\mathbf{Q} = \begin{bmatrix} \mathbf{Q}_{pre} \\ \mathbf{Q}_0 \\ \mathbf{Q}_{post} \end{bmatrix}. \tag{27}$$

Here, $\mathbf{Q}_0$ denotes the $(\eta_{pre}+1)^{\text{th}}$ row of matrix $\mathbf{Q}$. We can thus rewrite (17) as

$$\begin{aligned} r_1[n] = (\mathbf{Q}_0\,\mathbf{f}_1)^*\, a_0[n] + (\mathbf{Q}_{pre}\,\mathbf{f}_1)^H\,\mathbf{a}_{pre}[n] \\ + (\mathbf{Q}_{post}\,\mathbf{f}_1)^H\,\mathbf{a}_{post}[n] + w_s[n], \end{aligned} \tag{28}$$

where $a_0 \triangleq a[n-n_0] = a[n-\eta_{pre}]$, $\mathbf{a}_{pre} \triangleq [a[n] \ldots a[n-\eta_{pre}-1]]^T$, $\mathbf{a}_{post} \triangleq [a[n-\eta_{pre}+1] \ldots a[n-L_t+1]]^T$. In order to achieve a low bit error rate (BER), we have to concentrate most of the energy of the overall CIR $\mathbf{Q}\,\mathbf{f}_1$ in a *single* high energy tap $\mathbf{Q}_0\,\mathbf{f}_1$, while keeping the residual ISI caused by the terms $(\mathbf{Q}_{pre}\,\mathbf{f}_1)\,\mathbf{a}_{pre}[n]$ and $(\mathbf{Q}_{post}\,\mathbf{f}_1)\,\mathbf{a}_{post}[n]$ in (28) as small as possible. This introduces the following constraint on the PEF coefficients $\mathbf{f}_1$:

$$\mathbf{f}_1^H\mathbf{Q}_{pre}^H\mathbf{Q}_{pre}\mathbf{f}_1 + \mathbf{f}_1^H\mathbf{Q}_{post}^H\mathbf{Q}_{post}\mathbf{f}_1 \le \alpha, \tag{29}$$

where α is a design parameter which imposes an upper bound for the amount of residual ISI at the receiver. One possible choice that leads to a desirable system performance (as shown in Section V) is to set $\alpha = \sigma_s^2$ in order to limit the ISI to be less than or equal to the *noise variance*.

Note that our design goal regarding the energy concentration in a single tap can also be interpreted in terms of the *signal-to-interference-plus-noise-ratio* (SINR) for each symbol:

$$\text{SINR} = \frac{\mathbf{f}_1^H\mathbf{Q}_0^H\mathbf{Q}_0\mathbf{f}_1}{\mathbf{f}_1^H\mathbf{Q}_{pre}^H\mathbf{Q}_{pre}\mathbf{f}_1 + \mathbf{f}_1^H\mathbf{Q}_{post}^H\mathbf{Q}_{post}\mathbf{f}_1 + \sigma_s^2}. \tag{30}$$

Clearly, by maximizing $\mathbf{f}_1^H\mathbf{Q}_0^H\mathbf{Q}_0\mathbf{f}_1$, while suppressing $\mathbf{f}_1^H\mathbf{Q}_{pre}^H\mathbf{Q}_{pre}\mathbf{f}_1 + \mathbf{f}_1^H\mathbf{Q}_{post}^H\mathbf{Q}_{post}\mathbf{f}_1$, we can increase the SINR, leading to a better (i.e., lower) BER.

3) Power Constraint: Further to the PSD constraints, we can also limit the normalized *average* transmission power by including the following constraint [9], [10]:

$$\mathcal{E}\{|s_1[k]|^2\} = \mathbf{f}_1^H\,\boldsymbol{\Upsilon}_1\,\mathbf{f}_1 \le P^{\max}, \tag{31}$$

where $P^{\max} > 0$ is fixed and $\boldsymbol{\Upsilon}_1$ is a Hermitian Toeplitz matrix with vector

$$[\varphi[0]\varphi[-N]\ldots\varphi[-N(L_f-1)]] \tag{32}$$

in its first row, where $\varphi[k] \triangleq \tilde{g}[k] * \tilde{g}[-k]$, cf. [9, App. A].

Combining our considerations regarding spectral mask, energy concentration, and average transmit power, the proposed PEF design based on Structure I in Fig. 1(a) is obtained as the optimal solution of the following optimization problem over *complex-valued* vector variable $\mathbf{f}_1$:

$$\begin{aligned} \max_{\mathbf{f}_1} \quad & \mathbf{f}_1^H\mathbf{Q}_0^H\mathbf{Q}_0\mathbf{f}_1 \\ \text{s.t.} \quad & \mathbf{f}_1^H\mathbf{Q}_{pre}^H\mathbf{Q}_{pre}\mathbf{f}_1 + \mathbf{f}_1^H\mathbf{Q}_{post}^H\mathbf{Q}_{post}\mathbf{f}_1 \le \alpha \\ & \lambda(\omega_1)\,\mathbf{f}_1^H\mathbf{d}(N\omega_1)\mathbf{d}^H(N\omega_1)\mathbf{f}_1 \le m(\Omega_1) \\ & \vdots \\ & \lambda(\omega_K)\,\mathbf{f}_1^H\mathbf{d}(N\omega_K)\mathbf{d}^H(N\omega_K)\mathbf{f}_1 \le m(\Omega_K) \\ & \mathbf{f}_1^H\,\boldsymbol{\Upsilon}_1\,\mathbf{f}_1 \le P^{\max}. \end{aligned} \tag{33}$$

Problem (33) is a *non-concave* maximization problem as the objective function $\mathbf{f}_1^H\mathbf{Q}_0^H\mathbf{Q}_0\mathbf{f}_1$ is *not* concave in $\mathbf{f}_1$. Thus, the standard gradient-based methods (cf. [17]) cannot be used to solve problem (33). Moreover, problem (33) has many nonlinear constraints. Therefore, it is difficult to solve. Nevertheless, we can find a *close-to-optimal* solution for optimization problem (33) using a semi-definite relaxation technique, as we will explain in Section IV.

B. Problem Formulation for Structure II

Next, we consider the transceiver structure in Fig. 1(b). From (16), we can rewrite (15) as

$$r_2[n] = (\mathbf{B}\,\mathbf{f}_2)^H\mathbf{a}[n] + w_s[n], \tag{34}$$

where $\mathbf{a}[n]$ is as in (18), $\mathbf{f}_2 \triangleq [f_2[0] \ldots f_2[L_f-1]]^H$, and $\mathbf{B}$ is an $L_t \times L_f$ matrix with its i^{th} row equal to the $(N(i-1)+1)^{\text{th}}$ row of an $L_b \times L_f$ *column-circulant* matrix with vector

$$[b[k_0]\ b[1+k_0]\ \ldots\ b[L_g+L_h-1+k_0]\ \mathbf{0}_{L_f-1}^T]^H$$

as its first column and $L_b \triangleq L_g + L_h + L_f + 2N - 4$.

The spectral mask constraint for Structure II can be expressed as in (20) for each $\mu = 1, \ldots, K$, where $\Phi_{s_2 s_2}(e^{j\omega})$ is similar to (21). However, we need to rewrite (22) as

$$\Phi_{\tilde{v}_2\tilde{v}_2}(e^{j\omega}) = \left|F_2(e^{j\omega})\right|^2\ \Phi_{\tilde{a}_2\tilde{a}_2}(e^{j\omega}) = \left|F_2(e^{j\omega})\right|^2. \tag{35}$$

Thus, the spectral mask constraints can be reformulated as

$$\lambda(\omega_\mu)\ \left|F_2(e^{j\omega_\mu})\right|^2\ \le\ m(\Omega_\mu), \quad \mu = 1, \ldots, K. \tag{36}$$

Again, we can ensure (36) by optimizing the PEF coefficients.

Comparing the spectral mask constraints in (36) and (23), we can expect that the latter is more restrictive. To explain this, we note that the power spectrum of the PEF in Structure I, i.e., $\left|F_1(e^{j\omega_\mu N})\right|^2$, is essentially *repeated* N times across the bandwidth, thus severely limiting the degrees of freedom for spectrum shaping. This repetition is caused by the fact that the up-sampler is located *after* the PEF in Structure I. This problem does not occur in Structure II since the up-sampler is located *before* the PEF. This leads to a major improvement in overall system performance when Structure II is used, as long as the PEF length L_f and the spreading factor N are *not* too small. We will discuss this issue in detail in Section V-C.

The spectral mask constraint in (36) can be written in vector form as

$$\lambda(\omega_\mu)\mathbf{f}_2^H\mathbf{d}(\omega_\mu)\mathbf{d}^H(\omega_\mu)\mathbf{f}_2\ \le\ m(\Omega_\mu), \quad \mu = 1, \ldots, K, \tag{37}$$

where $\mathbf{d}(\omega) \triangleq [1 \; e^{j\omega} \; e^{j\omega 2} \; \ldots \; e^{j\omega(L_f-1)}]^T$. On the other hand, by similar steps as in [9, App. A], we can show that the power constraint in Structure II is obtained as

$$\mathcal{E}\{|s_2[k]|^2\} = \mathbf{f}_2^H \, \boldsymbol{\Upsilon}_2 \, \mathbf{f}_2 \leq P^{\max}, \tag{38}$$

where $\boldsymbol{\Upsilon}_2$ is a Hermitian Toeplitz matrix with vector $[\varphi[0]\varphi[1] \ldots \varphi[(L_f-1)]]$ in its first row. We define $\mathbf{B}_0$ as a $1 \times L_f$ matrix which includes the $(\eta_{pre}+1)^{\text{th}}$ row of matrix $\mathbf{B}$. We also define $\mathbf{B}_{pre}$ and $\mathbf{B}_{post}$ as the sub-matrices of $\mathbf{B}$ containing the first η_{pre} and the last η_{post} rows of $\mathbf{B}$, respectively. Finally, we notice that the energy concentration for Structure II is defined similarly as in (29). Therefore, an optimal PEF design based on Structure II in Fig. 1(b) is obtained by solving the following optimization problem over *complex-valued* vector variable $\mathbf{f}_2$:

$$\begin{aligned} \max_{\mathbf{f}_2} \quad & \mathbf{f}_2^H \mathbf{B}_0^H \mathbf{B}_0 \mathbf{f}_2 \\ \text{s.t.} \quad & \mathbf{f}_2^H \mathbf{B}_{pre}^H \mathbf{B}_{pre} \mathbf{f}_2 + \mathbf{f}_2^H \mathbf{B}_{post}^H \mathbf{B}_{post} \mathbf{f}_2 \leq \alpha \\ & \lambda(\omega_1) \; \mathbf{f}_2^H \mathbf{d}(\omega_1) \mathbf{d}^H(\omega_1) \mathbf{f}_2 \leq m(\Omega_1) \\ & \vdots \\ & \lambda(\omega_K) \; \mathbf{f}_2^H \mathbf{d}(\omega_K) \mathbf{d}^H(\omega_K) \mathbf{f}_2 \leq m(\Omega_K) \\ & \mathbf{f}_2^H \; \boldsymbol{\Upsilon}_2 \, \mathbf{f}_2 \leq P^{\max}. \end{aligned} \tag{39}$$

We notice that problem (39) is also a non-convex quadratic optimization problem, similar to problem (33). Next, we will explain how we can solve these problems efficiently.

IV. Solution of the Formulated Optimization Problems

In this section, we provide an algorithm to find close-to-optimal solutions for optimization problems (33) and (39). We first rewrite these problems in equivalent real-valued representations and solve them by using semi-definite relaxation and semi-definite programming techniques.

A. Real-valued Representation

Recall that vectors $\mathbf{f}_1$ and $\mathbf{f}_2$ in optimization problems (33) and (39) are complex. However, not all optimization solvers support complex-valued variables. In this section, we rewrite problems (33) and (39) in equivalent *real-valued* forms. Let $\mathbf{x}_1$ and $\mathbf{y}_1$ denote the real and imaginary parts of vector $\mathbf{f}_1$. Similarly, let $\mathbf{x}_2$ and $\mathbf{y}_2$ denote the real and imaginary parts of vector $\mathbf{f}_2$. We have

$$\mathbf{f}_1 = \mathbf{x}_1 + j \, \mathbf{y}_1, \qquad \mathbf{f}_2 = \mathbf{x}_2 + j \, \mathbf{y}_2. \tag{40}$$

For notational simplicity, we define

$$\mathbf{z}_1 \triangleq \begin{bmatrix} \mathbf{x}_1 \\ \mathbf{y}_1 \end{bmatrix}, \qquad \mathbf{z}_2 \triangleq \begin{bmatrix} \mathbf{x}_2 \\ \mathbf{y}_2 \end{bmatrix}. \tag{41}$$

By using simple calculus, we can obtain $2L_f \times 2L_f$ *real-valued* matrices $\boldsymbol{\Psi}_0$, $\boldsymbol{\Psi}_{pre}$, $\boldsymbol{\Psi}_{post}$, $\boldsymbol{\Phi}_0$, $\boldsymbol{\Phi}_{pre}$, and $\boldsymbol{\Phi}_{post}$ from $\mathbf{Q}_0$, $\mathbf{Q}_{pre}$, $\mathbf{Q}_{post}$, $\mathbf{B}_0$, $\mathbf{B}_{pre}$, and $\mathbf{B}_{post}$ respectively, such that

$$\mathbf{f}_1^H \mathbf{Q}_0^H \mathbf{Q}_0 \mathbf{f}_1 = \mathbf{z}_1^T \boldsymbol{\Psi}_0 \mathbf{z}_1, \tag{42}$$

$$\mathbf{f}_1^H \mathbf{Q}_{pre}^H \mathbf{Q}_{pre} \, \mathbf{f}_1 = \mathbf{z}_1^T \boldsymbol{\Psi}_{pre} \mathbf{z}_1, \tag{43}$$

$$\mathbf{f}_1^H \mathbf{Q}_{post}^H \mathbf{Q}_{post} \, \mathbf{f}_1 = \mathbf{z}_1^T \boldsymbol{\Psi}_{post} \mathbf{z}_1, \tag{44}$$

and

$$\mathbf{f}_2^H \mathbf{B}_0^H \mathbf{B}_0 \mathbf{f}_2 = \mathbf{z}_2^T \boldsymbol{\Phi}_0 \mathbf{z}_2, \tag{45}$$

$$\mathbf{f}_2^H \mathbf{B}_{pre}^H \mathbf{B}_{pre} \, \mathbf{f}_2 = \mathbf{z}_2^T \boldsymbol{\Phi}_{pre} \mathbf{z}_2, \tag{46}$$

$$\mathbf{f}_2^H \mathbf{B}_{post}^H \mathbf{B}_{post} \, \mathbf{f}_2 = \mathbf{z}_2^T \boldsymbol{\Phi}_{post} \mathbf{z}_2. \tag{47}$$

We can also obtain $2L_f \times 2L_f$ *real-valued* matrices $\boldsymbol{\Gamma}_1(\omega_\mu)$ and $\boldsymbol{\Gamma}_2(\omega_\mu)$, for each $\mu = 1, \ldots, K$, such that we have

$$\lambda(\omega_\mu) \; \mathbf{f}_1^H \; \mathbf{d}(N\omega_\mu) \, \mathbf{d}^H(N\omega_\mu) \, \mathbf{f}_1 = \mathbf{z}_1^T \; \boldsymbol{\Gamma}_1(\omega_\mu) \, \mathbf{z}_1, \tag{48}$$

$$\lambda(\omega_\mu) \; \mathbf{f}_2^H \; \mathbf{d}(\omega_\mu) \, \mathbf{d}^H(\omega_\mu) \, \mathbf{f}_2 = \mathbf{z}_2^T \; \boldsymbol{\Gamma}_2(\omega_\mu) \, \mathbf{z}_2. \tag{49}$$

In a similar way, we can obtain $2L_f \times 2L_f$ *real-valued* matrices $\boldsymbol{\Lambda}_1$ and $\boldsymbol{\Lambda}_2$ such that

$$\mathbf{f}_1^H \; \boldsymbol{\Upsilon}_1 \, \mathbf{f}_1 = \mathbf{z}_1^T \boldsymbol{\Lambda}_1 \mathbf{z}_1, \qquad \mathbf{f}_2^H \; \boldsymbol{\Upsilon}_2 \, \mathbf{f}_2 = \mathbf{z}_2^T \boldsymbol{\Lambda}_2 \mathbf{z}_2. \tag{50}$$

We are now ready to rewrite problem (33) as the following problem over *real-valued* variables:

$$\begin{aligned} \max_{\mathbf{z}_1} \quad & \mathbf{z}_1^T \boldsymbol{\Psi}_0 \mathbf{z}_1 \\ \text{s.t.} \quad & \mathbf{z}_1^T \, (\boldsymbol{\Psi}_{pre} + \boldsymbol{\Psi}_{post}) \, \mathbf{z}_1 \leq \alpha, \\ & \mathbf{z}_1^T \; \boldsymbol{\Gamma}_1(\omega_\mu) \, \mathbf{z}_1 \leq m(\Omega_\mu), \qquad \mu = 1, \ldots, K, \\ & \mathbf{z}_1^T \; \boldsymbol{\Lambda}_1 \, \mathbf{z}_1 \leq P^{\max}. \end{aligned} \tag{51}$$

We note that problems (33) and (51) are *equivalent*. In fact, their solutions can be converted into each other through the relationship in (40). They are also both non-concave problems.

We can also rewrite problem (39) as the following problem over *real-valued* variables:

$$\begin{aligned} \max_{\mathbf{z}_2} \quad & \mathbf{z}_2^T \boldsymbol{\Phi}_0 \mathbf{z}_2 \\ \text{s.t.} \quad & \mathbf{z}_2^T \, (\boldsymbol{\Phi}_{pre} + \boldsymbol{\Phi}_{post}) \, \mathbf{z}_2 \leq \alpha, \\ & \mathbf{z}_2^T \; \boldsymbol{\Gamma}_2(\omega_\mu) \, \mathbf{z}_2 \leq m(\Omega_\mu), \qquad \mu = 1, \ldots, K, \\ & \mathbf{z}_2^T \; \boldsymbol{\Lambda}_2 \, \mathbf{z}_2 \leq P^{\max}. \end{aligned} \tag{52}$$

We notice that problems (51) and (52) have similar structures. In particular, they are both real-valued non-concave quadratic maximization problems. In the remainder of this section, we will explain how we can solve optimization problems (51) and (52) with an acceptable accuracy.

B. Semi-definite Relaxation

Consider problem (51) based on Structure I. We introduce a new real-valued matrix $\mathbf{W}_1$ as

$$\mathbf{W}_1 \triangleq \mathbf{z}_1 \, \mathbf{z}_1^T. \tag{53}$$

Clearly, matrix $\mathbf{W}_1$ is positive semi-definite (i.e., $\mathbf{W}_1 \succeq \mathbf{0}$) and has unit rank. We also note that for any $2L_f \times 2L_f$ Hermitian matrix $\mathbf{A}$, we have

$$\mathbf{z}_1^T \; \mathbf{A} \, \mathbf{z}_1 = \text{trace} \, (\mathbf{A} \, \mathbf{W}_1). \tag{54}$$

Therefore, problem (51) is equivalent to

$$\begin{aligned} \max_{\mathbf{W}_1 \succeq \mathbf{0}} \quad & \text{trace} \, (\boldsymbol{\Psi}_0 \, \mathbf{W}_1) \\ \text{s.t.} \quad & \text{trace} \, ((\boldsymbol{\Psi}_{pre} + \boldsymbol{\Psi}_{post}) \, \mathbf{W}_1) \leq \alpha, \\ & \text{trace} \, (\boldsymbol{\Gamma}_1(\omega_\mu) \, \mathbf{W}_1) \leq m(\Omega_\mu), \quad \mu = 1, \ldots, K, \\ & \text{trace}(\boldsymbol{\Lambda}_1 \, \mathbf{W}_1) \leq P^{\max}, \\ & \text{rank}(\mathbf{W}_1) = 1. \end{aligned} \tag{55}$$

Problem (55) is still as difficult as problem (51), due to the rank constraint $\text{rank}(\mathbf{W}_1) = 1$.

Next, we *discard* the rank constraint and consider the following *relaxed* optimization problem:

$$\begin{aligned} \underset{\mathbf{W}_1 \succeq \mathbf{0}}{\max} \quad & \text{trace}\left(\mathbf{\Psi}_0\, \mathbf{W}_1\right) \\ \text{s.t.} \quad & \text{trace}\left(\left(\mathbf{\Psi}_{pre} + \mathbf{\Psi}_{post}\right) \mathbf{W}_1\right) \leq \alpha, \\ & \text{trace}\left(\mathbf{\Gamma}_1(\omega_\mu)\, \mathbf{W}_1\right) \leq m(\Omega_\mu), \quad \mu = 1, \ldots, K, \\ & \text{trace}(\mathbf{\Lambda}_1\, \mathbf{W}_1) \leq P^{\max}. \end{aligned} \tag{56}$$

Problem (56) is a *semi-definite programming* (SDP) problem [18]. SDP is a generalization of *linear programming* (LP) over matrices (rather than vectors as in LP). Several solvers, such as SeDuMi [19] can efficiently solve the SDP problem in (56). In Section IV-C, we will explain how solving problem (56) can help us find close-to-optimal solutions for problem (55).

In a similar way, we can introduce $\mathbf{W}_2 \triangleq \mathbf{z}_2\, \mathbf{z}_2^T$ and obtain the SDP relaxation of optimization problem (52) over real-valued matrix variable $\mathbf{W}_2$ based on Structure II.

C. PEF Design Algorithm

Let $\mathbf{W}_1^\star$ denote the optimal solution for SDP problem (56). If $\text{rank}(\mathbf{W}_1^\star) = 1$, then the solution $\mathbf{z}_1^\star$ for problem (55) can be obtained by using *eigenvalue decomposition* of matrix $\mathbf{W}_1^\star$. If $\text{rank}(\mathbf{W}_1^\star) > 1$, then we can still obtain a close approximation of $\mathbf{z}_1^\star$ (and also for $\mathbf{x}_1^\star$ and $\mathbf{y}_1^\star$) by using the following steps which are based on the recent results in [20], [21]:

- **Step 1.** Using eigenvalue decomposition, obtain matrix $\mathbf{U}_1^\star$ such that $\mathbf{W}_1^\star = \mathbf{U}_1^\star\, \mathbf{U}_1^{\star T}$:

$$\mathbf{W}_1^\star = \mathbf{V}_1^{\star T}\, \mathbf{\Sigma}_1^\star\, \mathbf{V}_1^\star \quad \Rightarrow \quad \mathbf{U}_1^\star = \mathbf{V}_1^{\star T}\, \mathbf{\Sigma}_1^{\star \frac{1}{2}},$$

  where $\mathbf{V}_1^\star$ is a *unitary* matrix and matrix $\mathbf{\Sigma}_1^\star$ is *diagonal*.

- **Step 2.** Using eigenvalue decomposition, obtain unitary matrix $\mathbf{\Theta}_1^\star$ which can make $\mathbf{\Theta}_1^{\star T}\mathbf{U}_1^{\star T}\mathbf{\Psi}_0\mathbf{U}_1^\star\mathbf{\Theta}_1^\star$ *diagonal*:

$$\mathbf{U}_1^{\star T}\mathbf{\Psi}_0\mathbf{U}_1^\star = \mathbf{\Theta}_1^\star\mathbf{\Xi}_1^\star\mathbf{\Theta}_1^{\star T} \;\Rightarrow\; \mathbf{\Xi}_1^\star = \mathbf{\Theta}_1^{\star T}\mathbf{U}_1^{\star T}\mathbf{\Psi}_0\mathbf{U}_1^\star\mathbf{\Theta}_1^\star,$$

  where $\mathbf{\Xi}_1^\star$ is a *diagonal* matrix.

- **Step 3.** Let ζ_i, $i = 1, \ldots, 2L_f$, be i.i.d. random variables taking values -1 and $+1$ with equal probabilities. Also, let $\boldsymbol{\zeta} = (\zeta_1, \ldots, \zeta_{2L_f})$. We select

$$\mathbf{z}_1^\star = \begin{bmatrix} \mathbf{x}_1^\star \\ \mathbf{y}_1^\star \end{bmatrix} = \frac{1}{\kappa_{\max}} \mathbf{U}_1^\star\, \mathbf{\Theta}_1^\star\, \boldsymbol{\zeta}, \tag{57}$$

  where

$$\kappa_{\max} = \max\left\{ \max_{1\leq\mu\leq K} \frac{\boldsymbol{\zeta}^T\, \mathbf{\Theta}_1^{\star T}\, \mathbf{U}_1^{\star T}\, \mathbf{\Gamma}_1(\omega_\mu)\, \mathbf{U}_1^\star\, \mathbf{\Theta}_1^\star\, \boldsymbol{\zeta}}{m(\Omega_\mu)}, \right.$$
$$\frac{\boldsymbol{\zeta}^T\, \mathbf{\Theta}_1^{\star T}\, \mathbf{U}_1^{\star T}\, \mathbf{\Lambda}_1\, \mathbf{U}_1^\star\, \mathbf{\Theta}_1^\star\, \boldsymbol{\zeta}}{P^{\max}},$$
$$\left. \frac{\boldsymbol{\zeta}^T \mathbf{\Theta}_1^{\star T} \mathbf{U}_1^{\star T}\, (\mathbf{\Psi}_{pre} + \mathbf{\Psi}_{post}) \mathbf{U}_1^\star \mathbf{\Theta}_1^\star \boldsymbol{\zeta}}{\alpha} \right\}.$$

  We can verify that for any random choice of vector $\boldsymbol{\zeta}$, the obtained $\mathbf{x}_1^\star$ and $\mathbf{y}_1^\star$ in (57) satisfy all inequality constraints in problem (51). We then set $\mathbf{f}_1^\star = \mathbf{x}_1^\star + j\, \mathbf{y}_1^\star$.

Let $\mathbf{f}_{1,opt}$ denote the optimal solution of the PEF design optimization problem in (33). We have

$$\mathbf{f}_1^{\star H}\mathbf{Q}_0^H\mathbf{Q}_0\mathbf{f}_1^\star \leq \mathbf{f}_{1,opt}^H\mathbf{Q}_0^H\mathbf{Q}_0\mathbf{f}_{1,opt} \leq \text{trace}\left(\mathbf{\Psi}_0\mathbf{W}_1^\star\right), \tag{58}$$

where the last inequality is valid because problem (56) is *less restrictive* than problem (33). From (58), the *optimality loss* when using $\mathbf{f}_1^\star$ instead of $\mathbf{f}_{1,opt}$ is upper-bounded as

$$\begin{aligned} \frac{\mathbf{f}_{1,opt}^H\mathbf{Q}_0^H\mathbf{Q}_0\mathbf{f}_{1,opt} - \mathbf{f}_1^{\star H}\mathbf{Q}_0^H\mathbf{Q}_0\mathbf{f}_1^\star}{\mathbf{f}_{1,opt}^H\mathbf{Q}_0^H\mathbf{Q}_0\mathbf{f}_{1,opt}} &= 1 - \frac{\mathbf{f}_1^{\star H}\mathbf{Q}_0^H\mathbf{Q}_0\mathbf{f}_1^\star}{\mathbf{f}_{1,opt}^H\mathbf{Q}_0^H\mathbf{Q}_0\mathbf{f}_{1,opt}} \\ &\leq 1 - \frac{\mathbf{f}_1^{\star H}\mathbf{Q}_0^H\mathbf{Q}_0\mathbf{f}_1^\star}{\text{trace}\left(\mathbf{\Psi}_0\mathbf{W}_1^\star\right)}. \end{aligned} \tag{59}$$

By using the upper bound in (59), we have verified through simulations (see Section V-B) that the optimality loss for the proposed design algorithm is small (less than 0.1%) in almost all simulated scenarios. Thus, a PEF design based on coefficients $\mathbf{f}_1^\star$ has *almost* the same performance as that achieved with the optimal coefficients $\mathbf{f}_{1,opt}$. Moreover, by following the analysis in [22], we can show that the optimality loss is *always* guaranteed to be less than 36%.

In a similar way, we can revise the three algorithmic steps above to obtain close-to-optimal solutions $\mathbf{f}_2^\star$ for optimization problem (39) for Structure II. Furthermore, we can show that

$$\frac{\mathbf{f}_{2,opt}^H\mathbf{B}_0^H\mathbf{B}_0\mathbf{f}_{2,opt} - \mathbf{f}_2^{\star H}\mathbf{B}_0^H\mathbf{B}_0\mathbf{f}_2^\star}{\mathbf{f}_{2,opt}^H\mathbf{B}_0^H\mathbf{B}_0\mathbf{f}_{2,opt}} \leq 1 - \frac{\mathbf{f}_2^{\star H}\mathbf{B}_0^H\mathbf{B}_0\mathbf{f}_2^\star}{\text{trace}\left(\mathbf{\Phi}_0\mathbf{W}_2^\star\right)}, \tag{60}$$

where $\mathbf{f}_{2,opt}$ denotes the optimal solution of the PEF design problem in (39) and $\mathbf{W}_2^\star$ denotes the solution obtained from the corresponding semi-definite relaxation. The inequality in (60) provides an upper bound on the optimality loss of our proposed design in Structure II.

V. Simulation Results

In this section, we assess the performance of our proposed PEF structures via simulations. We compare them with pure all-pre-Rake combining (*without* pre-equalization) [1], [6]–[8], the *symbol-level* minimum mean squared error (MMSE) pre-equalizer [9], and the *chip-level* MMSE pre-equalizer [10]. Unless stated otherwise, our simulation setting is as follows. The operational bandwidth is $B_s = 2\pi \times 1$ GHz with $\Omega_{\min} = 2\pi \times 3.5$ GHz and $\Omega_{\max} = 2\pi \times 4.5$ GHz [2], i.e., $K = 1001$. We use channel model CM1. We set the filter length to $L_f = 10$, the spreading factor to $N = 6$, the maximum transmit power to $P^{\max} = 1$, $\eta_{pre} = \eta_{post} = \lfloor \frac{L_t}{2} \rfloor$, and $\alpha = \sigma_s^2$.

A. Performance Comparison

Simulation results for the achieved BER for various pre-filter designs are shown in Fig. 3. Here, we consider channel models CM1 (solid lines) and CM4 (dashed-dotted lines). The length of the CIRs for channel model CM1 and CM4 are $L_h = 50$ and $L_h = 360$, respectively [12], [13]. We applied an appropriate power back-off in the cases where only the all-pre-Rake filter, the symbol-level MMSE PEF, and the chip-level MMSE PEF are used to avoid violating the spectral mask constraints. Note that no power back-off is needed for our

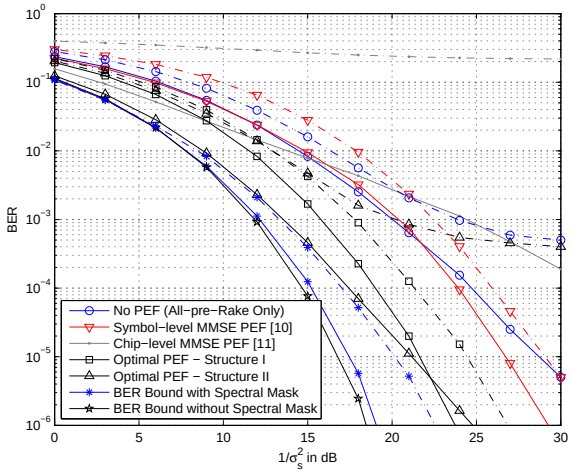

Fig. 3. BER vs. SNR $\frac{1}{\sigma_s^2}$ for all-pre-Rake filter, e.g., [1], (*with* power back-off), symbol-level MMSE PEF [9] (*with* power back-off), chip-level MMSE PEF [10] (*with* power back-off), and our proposed optimal PEF designs: Structure I and Structure II. Solid and dash-dotted lines indicate the simulation results for channel models CM1 and CM4, respectively.

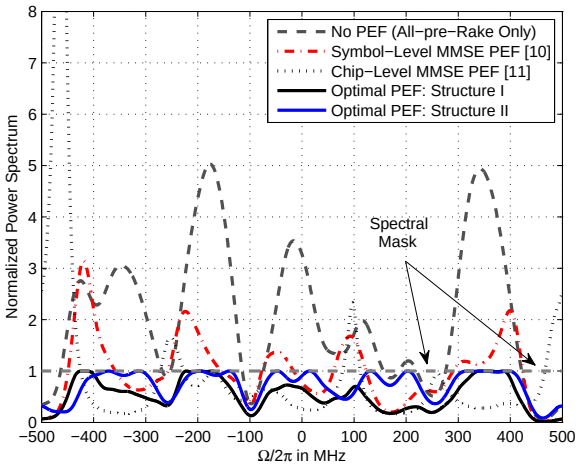

Fig. 4. Power spectrum of the transmitted UWB signals in baseband representation within $B_s = 2\pi \times 1$ GHz bandwidth for the all-pre-Rake filter (*without* power back-off), symbol-level MMSE PEF [9] (*without* power back-off), chip-level MMSE PEF [10] (*without* power back-off), and our proposed optimal PEF designs: Structure I and Structure II. Channel model is CM1.

optimal designs as we take the spectral mask into account in the PEF optimization. Let us first consider the results for channel model CM1. We can see that our designed optimal PEFs significantly improve the BER compared to the case where no PEF is included at the transmitter [1], [6]–[8], as well as to the cases where the MMSE PEF designs *without* spectral mask consideration are used [9], [10]. The performance is relatively poor for the MMSE PEFs as the designed filters (both at symbol-level and at chip-level) require major power back-off to meet the spectral mask before they can be used. The performance for the case with no PEF is also poor due to not only the impact of the power back-off, but also the negative impact of the residual ISI since the receiver does not include an equalizer. Next, consider the results for channel model CM4. Similar to the CM1 case, we can see that Structure II outperforms Structure I and all other design approaches when the SNR is low. However, since there are more residual ISI for CM4 than CM1, for CM4 Structure II performs poorly at high SNRs where ISI is the dominant binding factor. Interestingly, the chip-level MMSE PEF's performance is very poor as well in this case confirming the ISI limitation of short chip-level filters. While the performance of Structure II can be improved by increasing the filter length L_f and spreading factor N (see, e.g., Section V-C and Section V-D), we can see in Fig. 3 that Structure I even with the current filter length is capable of significantly reducing the BER and outperforming all other design schemes, including the symbol-level MMSE PEF [9].

For the results in Fig. 3, we have also included the BER bounds with and without spectral mask for both channel models CM1 and CM4. For the BER bounds *with* spectral mask, we assume that the optimum all-pre-Rake filter and an optimum PEF based on Structure II with a large number of coefficients (i.e., $L_f = 50$) and without the ISI suppression constraint are used at the transmitter and we ignore *any* ISI caused at the receiver. The BER bound *without* spectral mask is identical to the *matched-filter bound* which can be shown to be the same for both CM1 and CM4 [9]. We can see that the obtained BER for the proposed PEF designs, in particular the BER for Structure II when channel model CM1 is simulated and the BER for Structure I when channel model CM4 is simulated, are close to the idealized BER bounds, and the gap can be further reduced by increasing parameters L_f and N.

The power spectrum of the transmitted baseband UWB signals for various design schemes are shown for a random realization of CM1 in Fig. 4 (using a spectral oversampling factor of four corresponding to 4004 frequency points). Here, we normalized the spectral mask level to one for simplicity. We only included the results for channel model CM1. We can see that our designed optimal PEFs lead to transmitted signal power spectra that fully obey the spectral mask. In multiple frequency ranges (e.g., from 300 to 400 MHz for Structure II) the UWB transmit signal power spectrum lies on the unit-level line, approaching the shape of the spectral mask. On the other hand, the all-pre-Rake filter as well as the MMSE PEFs significantly violate the spectral mask within large portions of the operational frequency bandwidth. For the results shown in Fig. 4, the transmit power has to be down-scaled approximately by factors of 5, 3, and 12 for pre-Rake combining without PEF, the symbol-level MMSE PEF, and the chip-level MMSE PEF, respectively. Note that the spectral mask we considered here is *flat* as we focused on the typical UWB frequency range shown in Fig. 2. An example for a spectral mask which is *not* flat will be studied in Section V-F.

B. Optimality

Recall that the semi-definite relaxation in Section IV-B may lead to some loss in optimality in our PEF designs with respect to solving the original problems (33) and (39). In general, it is difficult to obtain the exact loss in optimality in each simulated scenario. However, the inequalities in (59) and (60) can help to obtain *upper bounds* on loss in optimality. Results are shown in Fig. 5 for 100 random channel realizations. We can see

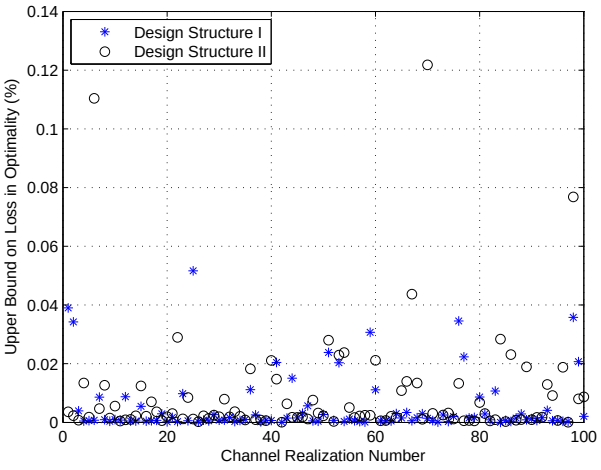

Fig. 5. Upper bounds on the loss of optimality in our proposed PEF design Structures I and II with respect to solving optimization problems (33) and (39), respectively. Here, we show the results for 100 random channel realizations.

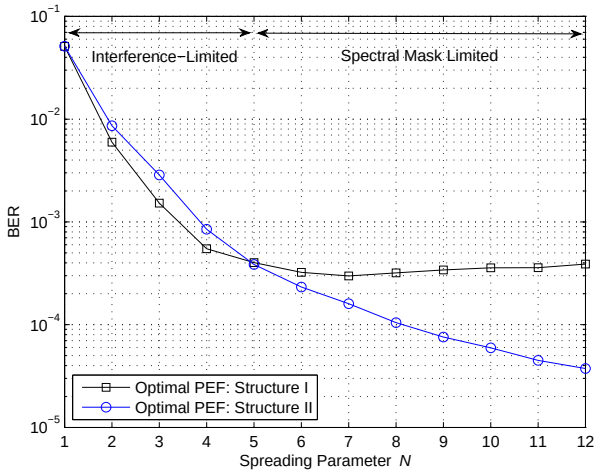

Fig. 6. Measured BER for Structure I and Structure II when the spreading factor N varies from 1 to 12 for filter length $L_f = 5$.

that our designs are very close to optimal for all cases. In most cases, the loss in optimality is less than 0.1%.

C. Design Trade-off

From the results in Fig. 3, although Structure II outperforms Structure I for SNR values less than 21 dB, it has inferior performance for higher SNRs. This suggests that there is a trade-off involved in determining which design structure is superior. In Fig. 6, we compare Structures I and II, where $\frac{1}{\sigma_s^2} = 18$ dB, PEF length $L_f = 5$, and the spreading factor N varies from 1 to 12. We can see that as N increases, the detection accuracy at the receiver monotonically improves for Structure II. This is because the second structure mostly suffers from residual ISI (as the degraded performance for high SNR values in Fig. 3 also suggests, especially for CM4). Therefore, additional spreading is helpful to reduce the residual ISI and to improve the BER. On the other hand, the performance of Structure I becomes quickly saturated as N increases and even slightly degrades for $N > 6$. This phenomenon does *not* occur in most communication systems where spreading is used. The results in Fig. 6 imply that if the PEF length L_f as well as the spreading factor N are small, then the first design structure works better than the second one. However, as the spreading factor increases, then it is Structure II which is preferred.

To explain why the BER starts increasing in Structure I as N grows, we look at the power spectrum for each PEF design for a sample channel realization in Fig. 7. Recall that the spectral mask constraints are as in (23) and (36) for Structure I and Structure II, respectively. For Structure I, the product $\lambda(\omega_\mu) \left|F_1(e^{j\omega_\mu N})\right|^2$ forms the transmit signal spectrum at frequency ω_μ, where $\mu = 1, \ldots, K$. On the other hand, for Structure II, the product $\lambda(\omega_\mu) \left|F_2(e^{j\omega_\mu})\right|^2$ forms the transmit signal spectrum. Considering the shapes of $\left|F_1(e^{j\omega_\mu N})\right|^2$ and $\left|F_2(e^{j\omega_\mu})\right|^2$ in Fig. 7, we can see that the power spectrum for the designed PEF is essentially *repeated* $N = 6$ times across the operational bandwidth for Structure I. This repetition is caused by the fact that the up-sampling unit is located *before*

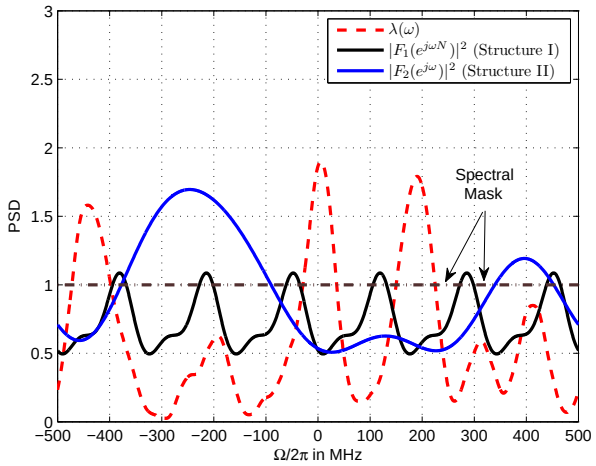

Fig. 7. Power spectral density of the optimal PEF for Structures I and II, when $L_f = 5$, and the PSD of the all-pre-Rake filter.

the PEF. As a result, any changes we make in the shape of the power spectrum of $\left|F_1(e^{j\omega_\mu N})\right|^2$, affect six different points on the transmit signal spectrum $\lambda(\omega_\mu) \left|F_1(e^{j\omega_\mu N})\right|^2$ within the bandwidth. Therefore, as N increases, it becomes more difficult for the PEF in Structure I to obey the spectral mask at all frequencies without degrading the overall system performance and increasing the BER. This explains why the performance is saturated and starts getting worse when N increases for Structure I in Fig. 6.

D. Complexity

Although we tackled the non-convexity in optimization problems (33) and (39) by using a semi-definite relaxation technique in Section IV-B, solving the resulting semi-definite programs can still be time consuming due to the large number of spectral mask constraints. For example, when the system bandwidth is $B_s = 2\pi \times 1$ GHz, problems (33) and (39) include $K = 1001$ spectral mask constraints. In this section, we examine the *performance-complexity* trade-off involved when we reduce the number of constraints. The simulation

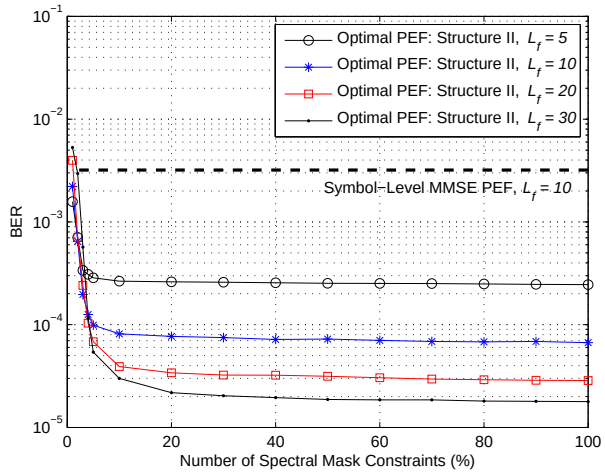

(a) BER

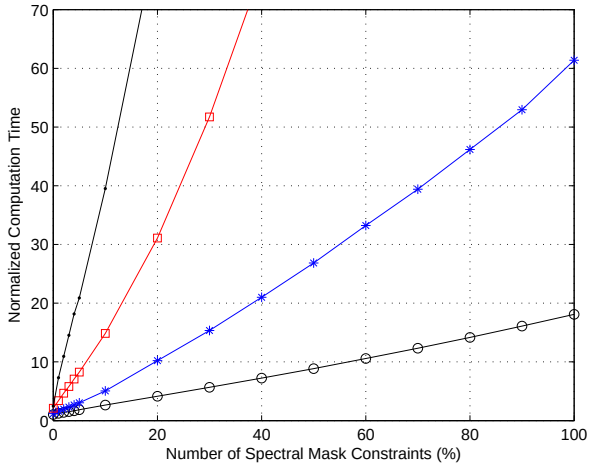

(b) Computation Time

Fig. 8. Impact of the choice of filter length L_f as well as the number of included spectral mask constraints on *performance-complexity* tradeoff. Here, we show the results only for Structure II when $N = 6$ and $\frac{1}{\sigma_s^2} = 18$ dB.

results are shown in Fig. 8, where $\frac{1}{\sigma_s^2} = 18$ dB and we include between 1% and 100% of the spectral mask constraints for various PEF length in Structure II. In this figure, the computation time is normalized with respect to the computation time for the symbol-level MMSE PEF design ($L_f = 10$) in [9] in order to have a platform-independent comparison. The spectral mask constraints are always at frequencies which *uniformly* spread out over bandwidth B_s. For example, if only 10% of the constraints are included in the PEF design optimization problems, they are located at frequencies $\mu_1, \mu_{11}, \ldots, \mu_{991}, \mu_{1001}$. Clearly, in this case, the power spectrum of the transmitted signal *may* violate the spectral mask at *other* frequencies, e.g., at $\mu_2, \ldots \mu_{10}$. This requires applying an appropriate *power back-off*, when needed. As a result, the performance degrades when fewer constraints are included. However, using fewer constraints can significantly reduce the computation time as shown in Fig. 8(b), making the designs more suitable in practice. Interestingly, no performance degradation is observed in Fig. 8(a) as long as we include at least 20% of the spectral

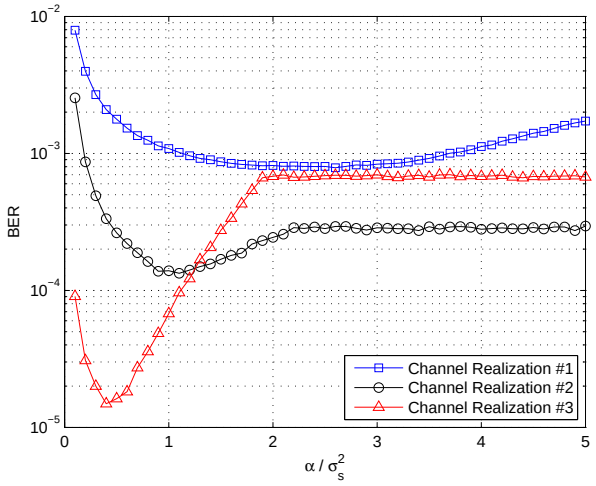

Fig. 9. The impact of the choice of parameter α on the BER for three random channel realizations when Structure II is simulated. The performance for the proposed PEF can be further improved by optimizing parameter α.

mask constraints. This is because the power spectrum is usually *smooth*. Moreover, in many cases for a *given complexity*, a better performance can be achieved by using *longer filters* with *fewer constraints*. For example, if we set $L_f = 20$ and include only 10% of the spectral mask constraints, we can reduce the BER by a factor of 10, compared to the case that we set $L_f = 5$ and include all spectral mask constraints. The computation time is even longer in the latter case. The results for Structure I are similar and are omitted for brevity.

E. Impact of Design Parameter α

The performance of the designed PEFs can be further improved if we optimize the residual ISI limit α in (29). This is shown in Fig. 9, where we plotted the resulting BER versus normalized α, for three random channel realizations for Structure II, where $\frac{1}{\sigma_s^2} = 18$ dB. We can see that the choice of $\alpha = \sigma_s^2$ is optimal for the second channel realization. However, changing α to $2.5\,\sigma_s^2$ and $\frac{\sigma_s^2}{2}$ can improve the performance for the first and the third channel realizations, respectively. Of course, this comes at the cost of extra computational complexity. Therefore, a fixed α is usually more appropriate in practice. Similar results can be obtained for Structure I.

F. Arbitrary Spectral Mask

In all simulation scenarios so far, we have assumed that the UWB system operates within its typical frequency range where the spectral mask is *flat*. In this section, we show that our PEF designs, particularly for Structure II, are flexible enough to be accommodated in any arbitrary spectral mask. As an example, consider the spectral mask shown in Fig. 10. For the results in this figure, we set the PEF length to $L_f = 30$ and the spreading factor to $N = 9$. In this example, the spectral mask includes a *notch* within the -100 MHz to 100 MHz baseband frequency range. As a possible practical scenario, this frequency range could have been reserved for the transmissions of a certain close-by incumbent legacy system in a cognitive radio scenario [23]. Fig. 10 shows that the Structure II can still nicely take

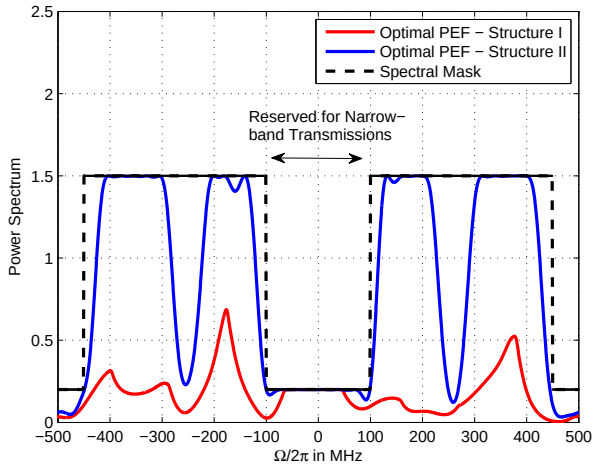

Fig. 10. Power spectrum for an arbitrary spectral mask with a notch indicating a frequency range in the middle of the operational bandwidth which is primarily reserved for nearby incumbent legacy narrow-band transmissions.

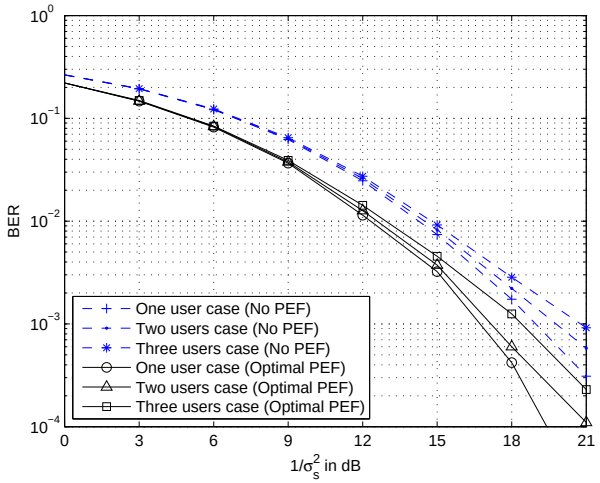

Fig. 11. BER vs. SNR $\frac{1}{\sigma_s^2}$ in the presence of multiple interfering users for the case that (i) all users employ an all-pre-Rake filter (matched to their own CIR in direction of the dedicated receiver) and (ii) all users employ our proposed optimal PEF design, Structure I (also matched to their own CIR).

on the shape of the spectral mask and exactly follow it at various frequencies. On the other hand, even Structure I is partly capable of following the changes in the imposed spectral mask; although it is not as flexible as Structure II. Similar results can be observed for other spectral mask shapes.

G. Multi-User Case

For simplicity of implementation, the proposed PEF design procedure in this paper was based on the single-user case. Extensions to the multi-user case seem feasible, but are outside the scope of this paper. Still, it is interesting to study the behavior of the proposed PEF transmitter structures in the presence of multiple interfering users. Fig. 11 presents BER results vs. SNR $\frac{1}{\sigma_s^2}$ in the presence of up to two interfering users (channel model CM2, BER results averaged over 100 CIR realizations) for the case that (i) all users employ an all-pre-Rake filter (matched to their own CIR in direction of the dedicated receiver) and (ii) all users employ our proposed optimal PEF design, Structure I (filter length $L_f = 10$, $B_s = 2\pi \times 1$ GHz, $K = 1001$; PEF also matched to own CIR in direction of the dedicated receiver). The CIRs associated with the interfering links were modeled statistically independent from those between the individual transmitters and the dedicated receivers. The spreading codes for the individual users were chosen according to [2], Table 6 ($N = 12$), where the user of interest was equipped with spreading code #3 and the interfering users with spreading codes #1 and #4. At the receiver of interest, the interfering signals were received with an attenuation of 10 dB compared to the desired signal. As can be seen, the performance degradation of the optimal PEF design in the presence of multiple users is similar to that in the case of pure all-pre-Rake combining. For example, at a BER of 10^{-3} a performance degradation of about 2 dB has to be accepted in the presence of two interfering links. Note, however, that the performance advantage of the optimal PEF design compared to the all-pre-Rake combining without a PEF (which is about 2 dB in this example at a BER of 10^{-3}) is preserved in the case of multi-user interference.

VI. Conclusions

We proposed a novel optimization-based PEF design framework for pre-Rake DS-UWB systems. Unlike the previous work on pre-equalizer and pre-Rake filter design in the literature, here we explicitly took into account the spectral mask constraints which are usually imposed by the telecommunications standardization and regulation bodies. As a result, our designs avoid the need for an inefficient power back-off, which is necessary for the previous pre-filter designs in order to meet the spectral mask constraints. We considered two different PEF design structures where the PEF is placed either *before* or *after* the up-sampling unit at the transmitter. We showed that the former works better in terms of reducing the residual inter-symbol interference, while the latter is more efficient in obeying the spectral mask. Therefore, each of the two designs can be superior versus the other one depending on the system parameters, particularly the choice of the spreading factor. Simulation results confirmed that both of the proposed PEF designs lead to significant performance gains over PEF structures without explicit spectral mask considerations. They have close-to-optimal performance with respect to the formulated optimization problems. Finally, both PEF designs have the capability of adhering to spectral masks with arbitrary shapes. In future work, our designs can be extended to the cases with other classes of design objectives as well as the use of multiple transmit and receive antennas. Moreover, it is interesting to extend our design to a multi-user scenario, where the design objective is to suppress not only the residual ISI but also the interference from other users while obeying the spectral mask.

References

[1] W. Cao, A. Nallanathan, and C. C. Chai, "A Novel High Data Rate Pre-rake DS UWB Multiple Access System: Interference Modeling and Trade-off between Energy Capture and Imperfect Channel Estimation Effect," *IEEE Trans. Wireless Commun.*, vol. 7, no. 9, pp. 3558–3567, 2008.

[2] R. Fisher, R. Kohno, M. McLaughlin, and M. Welbourn, "DS–UWB Physical Layer Submission to IEEE 802.15 Task Group 3a (Doc. Number P802.15-03/0137r4)," Jan. 2005.

[3] X. Wu, Z. Tian, T. N. Davidson, and G. B. Giannakis, "Optimal Waveform Design for UWB Radios," *IEEE Trans. Signal Processing*, vol. 54, no. 6, pp. 2009–2021, June 2006.
[4] M. Win and R. Scholtz, "Characterization of Ultra-Wide Bandwidth Wireless Indoor Channels: A Communication-Theoretic View," *IEEE J. Select. Areas Commun.*, vol. 20, pp. 1613–1627, Dec. 2002.
[5] T. Strohmer, M. Emami, J. Hansen, G. Papanicolaou, and A. Paulraj, "Application of Time-Reversal with MMSE Equalizer to UWB Communications," in *Proc. of IEEE Globecom*, Dallas, TX, Nov. 2004.
[6] H. Nguyen, I. Kovacs, and P. Eggers, "A Time Reversal Transmission Approach for Multiuser UWB Communications," *IEEE Trans. Antennas and Propagation*, vol. 54, pp. 3216–3224, Nov. 2006.
[7] R. Qiu, C. Zhou, N. Guo, and J. Zhang, "Time Reversal With MISO for Ultrawideband Communications: Experimental Results," *IEEE Antennas and Wireless Propagation Letters*, vol. 5, pp. 269–273, Dec. 2006.
[8] K. Usuda, H. Zhang, and M. Nakagawa, "Pre-Rake Performance for Pulse Based UWB System in a Standardized UWB Short-Range Channel," in *Proc. of IEEE WCNC*, Atlanta, GA, Mar. 2004.
[9] E. Torabi, J. Mietzner, and R. Schober, "Pre-Equalization for MISO DS-UWB Systems with Pre-Rake Combining," *IEEE Trans. Wireless Commun.*, vol. 8, pp. 1295–1307, Mar. 2009.
[10] M. Emami, M. Vu, J. Hansen, A. Paulraj, and G. Papanicolaou, "Matched Filtering with Rate Back–off for Low Complexity Communications in Very Large Delay Spread Channels," in *Proc. of Asilomar Conf. Sig, Sys., and Comp.*, Nov. 2004.
[11] F. Troesch, F. Althaus, and A. Wittneben, "Pulse position pre-coding exploiting UWB power constraints," in *Proc. IEEE Workshop on Signal Processing Adv. in Wireless Comm.*, Perugia, Italy, June 2005.
[12] "Channel Modeling Sub-Committee Final Report. IEEE 802.15-02/368r5-SG3a, IEEE P802.15," Dec. 2002.
[13] A. Molisch, J. Foerster, and M. Pendergrass, "Channel Models for Ultrawideband Personal Area Networks," *IEEE Wireless Communications*, vol. 10, pp. 14–21, Dec. 2003.
[14] "FCC Notice of Proposed Rule Making, Revision of Part 15 of the Commission's Rules Regarding Ultrawideband Transmission Systems," Communications Commission ET-Docket 98-153, May 2003.
[15] K. Witrisal, G. Leus, G. J. M. Janssen, M. Pausini, F. Troesch, T. Zasowski, and J. Romme, "Noncoherent Ultra-Wideband Systems," *IEEE Signal Processing Mag.*, vol. 26, no. 4, pp. 48–66, July 2009.
[16] A. Oppenheim and R. Schafer, *Digital Signal Processing*. Englewood Cliffs, New Jersey: Prentice–Hall, Inc., 1975.
[17] S. Boyd and L. Vandenberghe, *Convex Optimization*. Cambridge University Press, 2004.
[18] L. Vandenberghe and S. Boyd, "Semidefinite Programming," *SIAM Review*, vol. 38, pp. 49–95, Mar. 1996.
[19] I. Polik, "SeDuMi User Guide," http://sedumi.ie.lehigh.edu, June 2005.
[20] S. He, Z. Q. Luo, J. Nie, and S. Zhang, "Semidefinite Relaxation Bounds for Indefinite Homogeneous Quadratic Optimization," *SIAM Journal on Optimization*, vol. 19, pp. 503–523, June 2008.
[21] A. Nemirovski, C. Roos, and T. Terlaky, "On Optimization of Quadratic Form over Intersection of Ellipsoids with Common Center," *Mathematical Programming*, vol. 86, pp. 463–473, June 1999.
[22] Y. Nesterov, "Semidefinite Relaxation and Non-convex Quadratic Optimization," *Optimization Methods and Software*, vol. 12, pp. 1–20, 1997.
[23] S. Haykin, "Cognitive Radio: Brain-Empowered Wireless Communications," *IEEE J. Select. Areas Commun.*, vol. 23, pp. 201–220, Feb. 2005.

Amir-Hamed Mohsenian-Rad (S04-M09) received masters degree in Electrical Engineering from Sharif University of Technology in 2004 and Ph.D. degree in Electrical and Computer Engineering from The University of British Columbia (UBC) in 2008. Currently, he is an Assistant Professor in the Department of Electrical and Computer Engineering at Texas Tech University. Dr. Mohsenian-Rad is the recipient of the UBC Graduate Fellowship, Pacific Century Graduate Scholarship, and the Natural Sciences and Engineering Research Council of Canada (NSERC) Post-doctoral Fellowship. He is an Associate Editor of the International Journal of Electronics and Communication and serves as a Technical Program Committee member in various conferences, including IEEE Globecom, ICC, and CCNC. His research interests include design, optimization, and game-theoretic analysis of communication networks and smart power systems.

Jan Mietzner (S'02, M'08) was born in Rendsburg, Germany, on March 6, 1975. He studied electrical engineering at the Christian-Albrechts University (CAU) of Kiel, Germany, with focus on digital communications, and received the Dipl.-Ing. degree in July 2001. During his studies, he spent six months with the Global Wireless Systems Research Group, Lucent Technologies, Bell Labs U.K., in Swindon, England. For his diploma thesis on space-time codes he received the Prof.-Dr.- Werner-Petersen Award. From August 2001 to October 2006 he was with the Information and Coding Theory Lab (ICT), CAU Kiel, working toward his Ph.D. degree, which he received in December 2006. He received an award from the Friends of the Faculty of Engineering for the best dissertation in 2006. From January 2007 to December 2008 he was with the Department of Electrical and Computer Engineering, University of British Columbia, in Vancouver, Canada, as a post-doctoral research fellow sponsored by the German Academic Exchange Service (DAAD). His research interests concern physical layer aspects of future wireless communication systems, especially multiple-antenna techniques, ultra-wideband and cognitive radio systems, relaying, and cooperative diversity techniques. Dr. Mietzner received the 2009 best paper award from the German Information Technology Society (ITG). He has served as a TPC member for IEEE WCNC 2009 and 2010, Globecom 2009 and 2010, and ICC 2011 conferences. In March 2009, he joined EADS Germany, Defence and Security (now CASSIDIAN), in Ulm, Germany.

Robert Schober (M'01, SM'08, F'10) was born in Neuendettelsau, Germany, in 1971. He received the Diplom (Univ.) and the Ph.D. degrees in electrical engineering from the University of Erlangen-Nuermberg in 1997 and 2000, respectively. From May 2001 to April 2002 he was a Postdoctoral Fellow at the University of Toronto, Canada, sponsored by the German Academic Exchange Service (DAAD). Since May 2002 he has been with the University of British Columbia (UBC), Vancouver, Canada, where he is now a Full Professor and Canada Research Chair (Tier II) in Wireless Communications. His research interests fall into the broad areas of Communication Theory, Wireless Communications, and Statistical Signal Processing.

Dr. Schober received the 2002 Heinz MaierLeibnitz Award of the German Science Foundation (DFG), the 2004 Innovations Award of the Vodafone Foundation for Research in Mobile Communications, the 2006 UBC Killam Research Prize, the 2007 Wilhelm Friedrich Bessel Research Award of the Alexander von Humboldt Foundation, and the 2008 Charles McDowell Award for Excellence in Research from UBC. In addition, he received best paper awards from the German Information Technology Society (ITG), the European Association for Signal, Speech and Image Processing (EURASIP), IEEE ICUWB 2006, the International Zurich Seminar on Broadband Communications, and European Wireless 2000. Dr. Schober is also the Area Editor for Modulation and Signal Design for the IEEE Transactions on Communications.

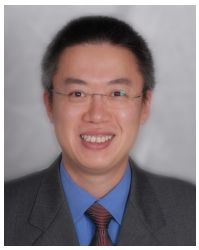

Vincent W.S. Wong (SM'07) received the B.Sc. degree from the University of Manitoba, Winnipeg, MB, Canada, in 1994, the M.A.Sc. degree from the University of Waterloo, Waterloo, ON, Canada, in 1996, and the Ph.D. degree from the University of British Columbia (UBC), Vancouver, BC, Canada, in 2000. From 2000 to 2001, he worked as a systems engineer at PMC-Sierra Inc. He joined the Department of Electrical and Computer Engineering at UBC in 2002 and is currently an Associate Professor. His research interests are in resource and mobility management for wireless mesh networks, wireless sensor networks, and heterogeneous wireless networks. Dr. Wong is an Associate Editor of the IEEE Transactions on Vehicular Technology and an Editor of KICS/IEEE Journal of Communications and Networks. He serves as TPC member in various conferences, including IEEE Infocom, ICC, and Globecom. He is a senior member of the IEEE and a member of the ACM.